KEMENTERIAN RISET, TEKNOLOGI DAN PENDIDIKAN TINGGI
UNIVERSITAS NEGERI SURABAYA
**FAKULTAS MATEMATIKA DAN ILMU PENGETAHUAN ALAM**

**Kampus Ketintang**
Jalan Ketintang Gedung D1
Surabaya 60231
Telepon : +6231-8296427
Email : info@fmipa.unesa.ac.id
Laman : fmipa.unesa.ac.id



# SURAT KETERANGAN

Nomer: B/34656/UN38.3/KP.18.31/2019

Pejabat yang bertanda-tangan di bawah ini adalah Dekan Fakultas Matematika dan Ilmu Pengetahuan Alam (FMIPA), Universitas Negeri Surabaya (Unesa) menerangkan dengan sesungguhnya bahwa:

| | |
|---|---|
| Nama Lengkap dengan gelar | : Tjipto Prastowo, Ph.D |
| NIP | : 196702031995021001 |
| NIDN | : 0003026702 |
| Pangkat / Golongan | : Pembina / IVa |
| Jabatan Fungsional | : Lektor Kepala |
| Unit Kerja | : FMIPA Unesa |

belum pernah memasukkan karya ilmiah berikut ini berupa publikasi internasional di jurnal bereputasi untuk kenaikan pangkat dan jabatan yang terakhir dengan rincian sebagai berikut:

| | |
|---|---|
| Judul Artikel | : Effects of topography on the cumulative mixing efficiency in exchange flows |
| Nama Jurnal | : Journal of Geophysical Research (JGR) |
| H-indeks dan Kategori Jurnal | : 280, Q1 by Schimago-JR |
| Cite Score | : 3,49 by Scopus |
| Nama Penerbit | : Wiley-Blackwell |
| E-ISSN | : 2156-2202 |
| Volume dan Nomer Artikel | : Vol. 114, C08008, doi: 10.1029/2008JC005152 http://onlinelibrary.wiley.com/doi/10.1029/2008JC005152/epdf |
| Bulan dan Tahun Terbit | : Agustus 2009 |

Demikian Surat Keterangan ini dibuat dengan sebenar-benarnya sebagai bagian dari Usulan Guru Besar atas nama dosen dengan nama lengkap di atas untuk dipergunakan sebagaimana mestinya.

Surabaya 27 Mei 2019
Dekan FMIPA,

KEMENTERIAN RISET, TEKNOLOGI, DAN PENDIDIKAN TINGGI UNIVERSITAS NEGERI SURABAYA UNESA FAKULTAS MATEMATIKA DAN ILMU PENGETAHUAN ALAM

Prof. Dr. Madlazim, M.Si.
NIP 196511051991031012

JOURNAL OF GEOPHYSICAL RESEARCH, VOL. 114, C08008, doi:10.1029/2008JC005152, 2009



# Effects of topography on the cumulative mixing efficiency in exchange flows

T. Prastowo,[1] R. W. Griffiths,[1] G. O. Hughes,[1] and A. M. Hogg[1]

Received 10 October 2008; revised 5 March 2009; accepted 3 June 2009; published 15 August 2009.

[1] Buoyancy-driven, hydraulically controlled two-layer exchange flows were established in a laboratory flume with a lateral constriction and a bottom sill placed at its midpoint. The shear flow was unstable within the constriction, and the overall amount of turbulent mixing was determined from measurements of vertical density profiles after the exchange. The potential energy changes are used to evaluate the mixing efficiency (or flux Richardson number), defined as the fraction of the available potential energy released into kinetic energy that is converted to potential energy through irreversible mixing. Mixing efficiencies asymptote at large Reynolds numbers to values of 8% for a sill with sloping sides and 11% ± 1% for both a weir with vertical sides and the same constriction with no bottom topography. The latter is identical to the value previously reported for shorter, smoothly varying lateral constrictions. Thus, all controlled exchanges examined here undergo less mixing than implied by the commonly assumed maximum turbulent mixing efficiency of 20%, and the actual efficiency is insensitive to the form of the topography. This result implies that calculations of the global energy balance of the ocean may need to be reevaluated.

**Citation:** Prastowo, T., R. W. Griffiths, G. O. Hughes, and A. M. Hogg (2009), Effects of topography on the cumulative mixing efficiency in exchange flows, *J. Geophys. Res.*, *114*, C08008, doi:10.1029/2008JC005152.

## 1. Introduction

[2] The relationship between energy input and the consequent amount of mixing is fundamental to understanding and modeling any turbulent stratified shear flow. Vertical mixing plays an important role in lake and estuary dynamics, and it is thought to be an important factor governing the strength of the global meridional overturning circulation of the oceans and the magnitude of the abyssal density stratification [*Munk and Wunsch*, 1998]. In the case of the global overturning circulation, both the amount of mixing required and the available energy input are poorly known [*Wunsch and Ferrari*, 2004]. More generally, the input power required to sustain a given rate of mixing in a stratified flow is uncertain. Here we use laboratory experiments with hydraulically controlled, buoyancy-driven exchange [*Farmer and Armi*, 1986] to examine mixing in stratified shear flows. These flows capture much of the essence of exchange flows common in the oceans, where straits or sills control the exchange of waters of differing densities between adjacent ocean basins or across abyssal topographic barriers, and where much mixing occurs [*Bryden and Nurser*, 2003]. Significantly, for this class of flows it is possible in the laboratory to make accurate measurements of both energy input and the cumulative amount of irreversible mixing [*Prastowo et al.*, 2008]. The results will also be more broadly relevant to shear-generated turbulent mixing.

[3] An important quantity characterizing stratified turbulent mixing is the mixing efficiency. This is variously defined. For stably stratified flows a common definition of efficiency is the fraction of the kinetic energy supplied to turbulence that is irreversibly converted into potential energy of the density field, the remainder being dissipated by viscosity [*Caulfield and Peltier*, 2000; *Peltier and Caulfield*, 2003]. This efficiency is equivalent to the flux Richardson number $Ri_f$, the ratio of the vertical buoyancy flux to the rate of production of turbulent kinetic energy by shear, if the buoyancy flux is entirely irreversible. For stably stratified shear flows $Ri_f > 0$. An alternative definition of mixing efficiency is $\Gamma = Ri_f/(1 - Ri_f)$, which represents the ratio of energy used for irreversible mixing relative to that dissipated by viscosity. *Osborn* [1980] proposed an asymptotic value of $\Gamma \approx 0.18$ (usually rounded to 0.2) as the upper bound, derived from a critical $Ri_f$ of 0.15 [*Ellison*, 1957] above which the turbulence cannot be sustained. This approximate upper bound is supported by laboratory experiments, which show that the mixing efficiency depends on turbulence Reynolds number and Froude number [*Ivey and Imberger*, 1991; *Ivey et al.*, 2008] or Richardson number [*Linden*, 1979, 1980], but has a maximum value $Ri_f \leq 0.25$ for shear generated mixing, $Ri_f \leq 0.12$ for turbulence generated by an oscillating grid [*Linden*, 1979], or an asymptote of $Ri_f \approx 0.20$ at sufficiently large turbulence Reynolds numbers for internal wave breaking on a slope [*Ivey and Imberger*, 1991]. Similar mixing efficiencies have been inferred from measurements in the upper ocean [*Gargett*

[1]Research School of Earth Sciences, Australian National University, Canberra, ACT, Australia.


0148-0227/09/2008JC005152$09.00

*and Moum*, 1995; *Moum*, 1996; *Ruddick et al.*, 1997]. Although mixing efficiencies can be much smaller than these values, the upper bound (commonly taken as $Ri_f \approx 0.2$) has been used as an estimate of the average efficiency of turbulent mixing in the oceans for the purpose of estimating the total power input required to achieve a designated rate of mixing in the interior of the ocean [*Munk and Wunsch*, 1998; *Webb and Suginohara*, 2001; *Wunsch and Ferrari*, 2004; *St. Laurent and Simmons*, 2006].

[4] Recent laboratory experiments [*Monti et al.*, 2007; *Patterson et al.*, 2006] have demonstrated that individual turbulent events associated with the growth and collapse of Kelvin-Helmholtz billows lead to time-dependent mixing, with the mixing efficiency approaching an asymptotic value at large times. Numerical simulations of the full life cycle of a Kelvin-Helmholtz billow during a transition from a laminar to a fully turbulent state [*Caulfield and Peltier*, 2000; *Peltier and Caulfield*, 2003] similarly show that the instantaneous mixing efficiency $Ri_f$ evolves and that, at late times, the time-averaged mixing efficiency approaches a value of 0.15. The averaged, or cumulative, mixing efficiency is the measure of greatest interest in geophysical applications.

[5] Other studies [*Stigebrandt and Aure*, 1989; *Arneborg*, 2002] have suggested that even smaller efficiencies, $Ri_f \approx 0.1$, are possible. In particular, when a turbulent mixing event generates a patch of mixed water in an initially linearly stratified ambient, the mixed water eventually spreads laterally to reach an equilibrium state. *Arneborg* [2002] defined the small-scale flux Richardson number ($\sim$0.2) to characterize the localized mixing within the turbulent patch, and a overall flux Richardson number to describe the whole mixing process. In the final state the irreversible increase in potential energy attributable to mixing is approximately one half of the increase calculated for the localized patch. Hence the overall flux Richardson number based on this final potential energy increase is approximately 0.1.

[6] In recent laboratory experiments with density-driven exchange between two reservoirs *Prastowo et al.* [2008] have demonstrated that it is possible to make accurate measurements of both the amount of shear-induced turbulent mixing and the energy available to turbulence. In the experiments, fluids of different densities were allowed to exchange through a lateral constriction after a barrier between two long reservoirs was removed. The flows were hydraulically controlled, strong vertical shear generated Kelvin-Helmholtz billows and an interfacial mixing region in the contraction, and the resulting mixed water was advected into the two reservoirs. By replacing the barrier to shut off the exchange flow before bores reflected from the far end walls, attention could be restricted to steady mean flow conditions in the mixing regions. The ratio of potential energy increase due to mixing, to the available potential energy released, was found to asymptote to a well-defined constant value of $0.11 \pm 0.01$ at large Reynolds numbers. This quantity is the cumulative mixing efficiency.

[7] Here we extend the methodology of *Prastowo et al.* [2008] to cases with bottom topography in the form of sills placed at the midpoint in the length of the lateral constriction. The mean flows are again steady and hydraulically controlled. The experimental methods, measurements and analysis techniques have been reported elsewhere and are therefore reviewed only briefly in section 2. We then compare measured mixing efficiencies for flow over topography with those for flows through simple lateral constrictions with no bottom topography.

## 2. Experimental Apparatus and Method

### 2.1. Apparatus

[8] The experiments used the same tank and apparatus of *Prastowo et al.* [2008]. A long channel of length $L = 5.26$ m and width $B = 0.2$ m, was divided into two equal reservoirs by placing a smoothly varying constriction and a removable sliding barrier at its midpoint (Figure 1). *Prastowo et al.* [2008] reported results for four different constrictions within which the channel width was decreased but there was no bottom topography. For sufficiently large Reynolds numbers the measured mixing efficiencies were not dependent on the constriction ratio $b_0/B$ ($b_0$ the minimum constriction width), the water depth $H$ or the length $L_c$ of the constriction. Here we chose the longest of those lateral constrictions (Figure 1a), having curved walls at its exits and a straight, parallel-sided central section of width 0.06 m and length 0.5 m (the total constriction length $L_c$ was 1.0 m). One of two different sills was placed at the midpoint of the constriction: a triangular sill with sloping sides (0.5 m long and 0.1 m high; Figure 1b), or a vertical weir (0.02 m thick and 0.1 m high; Figure 1c). Each sill was uniform across the constriction width.

[9] For each experiment, the tank was filled with freshwater to depth 0.2 m. The sliding vertical barrier was then inserted at the central point of the constriction, meeting the top of the sill. A density difference across the barrier was created by dissolving a measured mass of salt into one reservoir (the right hand side in the images shown in this paper). For flow visualisation, the two solutions were dyed with different colors. Both reservoirs were stirred thoroughly to ensure homogeneity in density. The free surface heights were subsequently adjusted to give equal hydrostatic pressures at middepth, so as to achieve a purely baroclinic exchange. The exchange flow was initiated by the smooth and rapid removal of the barrier from the water over a period lasting approximately 1 s. The barrier was rapidly reinserted into the channel at a time when the resulting gravity currents had nearly reached the end walls of the tank, thus ensuring that the finite length of the channel had no influence on the flow in the vicinity of the constriction. Run durations ranged from 15 s to 147 s. In other runs not detailed here, the exchange flow was stopped at various times before and after the initial gravity currents had reached the end walls. In cases where the barrier was replaced after the reflected waves from the end walls had arrived back at the constriction, the mean flow through the constriction became unsteady and was substantially modified by the interactions.

### 2.2. Measurement Techniques

[10] Before starting each exchange flow the initial densities of the fresh and saltwater reservoirs were sampled and measured in an Anton Paar digital density meter. The initial positions of the free surface in the fresh and saltwater reservoirs were determined (to within ±0.01 mm) using a digital micrometer gauge with an attached upward pointing needle point immersed in the water.

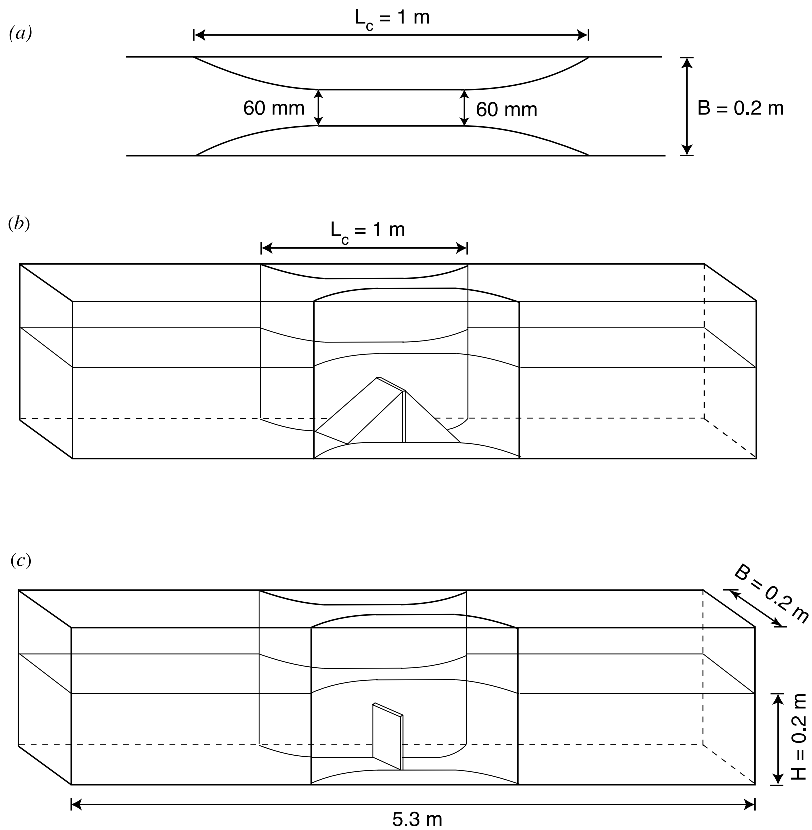


**Figure 1.** Experimental apparatus showing (a) the planform of the long lateral constriction and the geometry of (b) the triangular sill and (c) the weir.

[11] After the exchange flow was stopped the water was left to stand for at least 2 h, which was long enough for all long waves to die away but too short for diffusion of salt to affect the density distribution on length scales greater than 3 mm. During this time the top of the tank was sealed to minimize evaporation. Density profiles were measured by taking 20 samples from each reservoir using a rake of hypodermic sampling tubes spaced vertically at 10 mm intervals throughout the water depth. The density of each sample was measured using the digital density meter to a precision of $10^{-3}$ kg m$^{-3}$. The final free surface positions were also measured, as these were required in calculations of the final potential energy.

### 2.3. Experimental Conditions

[12] *Prastowo et al.* [2008] reported 30 experiments with shorter constrictions of various widths and nine runs with the same long constriction used here, but with no bottom topography. We carried out nine new experiments with the triangular sloping sill and six runs with the vertical weir. The relevant variables are the reduced gravity $g' = g\Delta\rho/\rho_2$ (where $g$ is acceleration due to gravity, $\Delta\rho/\rho_2 = (\rho_2 - \rho_1)/\rho_2$ is the fractional density difference and $\rho_1$ and $\rho_2$ are the initial densities of the fresh and saltwater reservoirs, respectively), the total water depth $H$, the minimum constriction width $b_o$, the constriction length $L_c$, the sill height $h_s$ and the kinematic viscosity $v$.

[13] The important dimensionless parameters that govern the flow are the flow aspect ratio $L_c/H$, the contraction aspect ratio $b_o/B$, the fractional sill height $h_s/H$ and a Reynolds number. *Prastowo et al.* [2008] argued that the most appropriate Reynolds number is one based on the length of the constriction, which is the length scale for flow acceleration. For a constriction with no bottom topography the velocities are approximately $0.5(g'H)^{1/2}$ and we define the "horizontal Reynolds number"

$$Re_L = \frac{0.5(g'H)^{1/2}L_c}{\nu}. \quad (1)$$

Given that the previous work examined the effects of constriction width and length, and water depth for the case of no topography, we here concentrate on the effects of topography. We vary only the density difference $\Delta\rho$ and topography shape. The horizontal Reynolds number for runs with the long constriction with no topography lay in the range $2.0 \times 10^4 \leq Re_L \leq 1.5 \times 10^5$. For runs with sills the fractional sill height was fixed at 0.5 and the constriction ratio was fixed at 0.30. The flow speed over the sills is assumed to scale with $0.5(g'H/2)^{1/2}$, as the water depth over the sill was $H/2$. For sill exchanges we use the horizontal Reynolds number $Re_L = 0.5(g'H/2)^{1/2}L_c/\nu$.

### 2.4. Analysis

[14] The density profiles $\rho'_1(z)$ and $\rho'_2(z)$ measured after the exchange flow can be used with conservation of the mass of salt to derive expressions for the mass exchanged

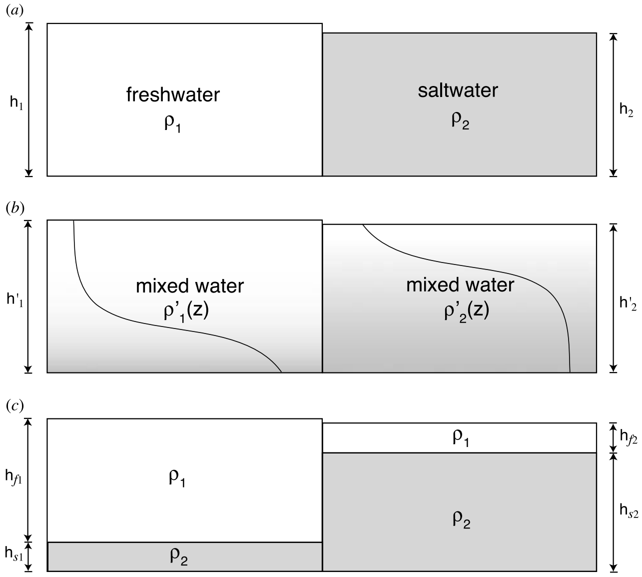


**Figure 2.** Representations of the density distributions in (a) the initial state, (b) the final state, and (c) the hypothetical nonmixing state.

(see section 4), the change in potential energy and the mixing efficiency. For the initial state with two homogeneous solutions of different density (Figure 2a), the gravitational potential energy of the water masses is given by

$$P_i = g\int_0^{h_1} A\rho_1 z\,dz + g\int_0^{h_2} A\rho_2 z\,dz, \quad (2)$$

where $h_1$ and $h_2$ are the initial free surface heights of the fresh and saltwater reservoirs, respectively, above the base of the reservoirs at $z = 0$ and $A$ is the horizontal cross section of each reservoir, which may be either uniform or dependent on height. The hypsometry of the topography, $A(z)$, must be taken into account in calculations.

[15] In the final state after the exchange flow and mixing have occurred (Figure 2b), the gravitational potential energy can be calculated from the measured density distribution in each reservoir,

$$P_f = g\int_0^{h'_1} A\rho'_1(z)z\,dz + g\int_0^{h'_2} A\rho'_2(z)z\,dz, \quad (3)$$

where $h'_1$ and $h'_2$ are the final free surface heights.

[16] In order to characterize the effect of mixing, we define the hypothetical final state that would be present if there had been no mixing during the exchange (but the same mass was transported). The potential energy of the actual final state (3) is greater than that of the hypothetical unmixed state. This hypothetical state is obtained by notionally redistributing the measured total amount of salt within each reservoir into fresh and saltwater layers of densities $\rho_1$ and $\rho_2$ (Figure 2c). The required thicknesses of the fresh and saltwater layers in each of the reservoirs for this state are $h_{fi}$ ($i$ = 1, 2) and $h_{si}$ ($i$ = 1, 2), respectively, where $h_{s1}$ and $h_{s2}$ are given by

$$h_{si} = \frac{1}{\rho_2 - \rho_1}\int_0^{h'_i}\left(\rho'_i(z) - \rho_1\right)dz. \quad (4)$$

We assume that the equation of state is linear, so that the total volume of the two reservoirs is constant and $h_{fi} = h'_i - h_{si}$, where $h'_i$ is the measured final water depth. The potential energy of the hypothetical state is given by

$$P_h = g\int_0^{h_{s1}} A\rho_2 z\,dz + g\int_{h_{s1}}^{h'_1} A\rho_1 z\,dz + g\int_0^{h_{s2}} A\rho_2 z\,dz + g\int_{h_{s2}}^{h'_2} A\rho_1 z\,dz. \quad (5)$$

[17] The amount of mixing, as measured by the resultant increase in potential energy $\Delta P_m$, is

$$\Delta P_m = P_f - P_h. \quad (6)$$

The amount of available potential energy $\Delta P_a$ released from the initial state into the exchange flow is the difference between the initial and hypothetical final (unmixed) states:

$$\Delta P_a = P_i - P_h. \quad (7)$$

[18] We define the mixing efficiency as that fraction of the available potential energy released to kinetic energy of the flow that is subsequently transformed irreversibly to increase the potential energy of the final density distribution above the hypothetical unmixed state. The efficiency $\eta$ becomes

$$\eta = \frac{\Delta P_m}{\Delta P_a} = \frac{P_f - P_h}{P_i - P_h}. \quad (8)$$

This definition (8) represents the overall efficiency with which mixing draws on the initial available energy, noting that $\Delta P_a$ is the total mechanical energy supplied.

## 3. Qualitative Observations

[19] After the barrier was removed, the exchange flow over the triangular sill was characterized by turbulent billow growth on the density interface and extensive mixing between the layers (Figure 3). Billows initially grew along the entire length of the constriction. The initial transient stage of the flow within the constriction took only about 5% of the total time allowed for the exchange. During this period the gravity current heads passed out of the constriction, stationary hydraulic jumps developed, the first generation of billows in the constriction grew and collapsed, and the interface reached a steady mean shape.

[20] When the flow had reached its quasi-steady condition (Figures 3c and 3d) billows were concentrated at the crest of the sill (where the two layers had equal depths), in the downslope flow region on the left hand side of the constriction, and in the expansion region at the far right hand end. These are the regions of flow acceleration, as indicated by the greater slope of the density interface. Along the region of

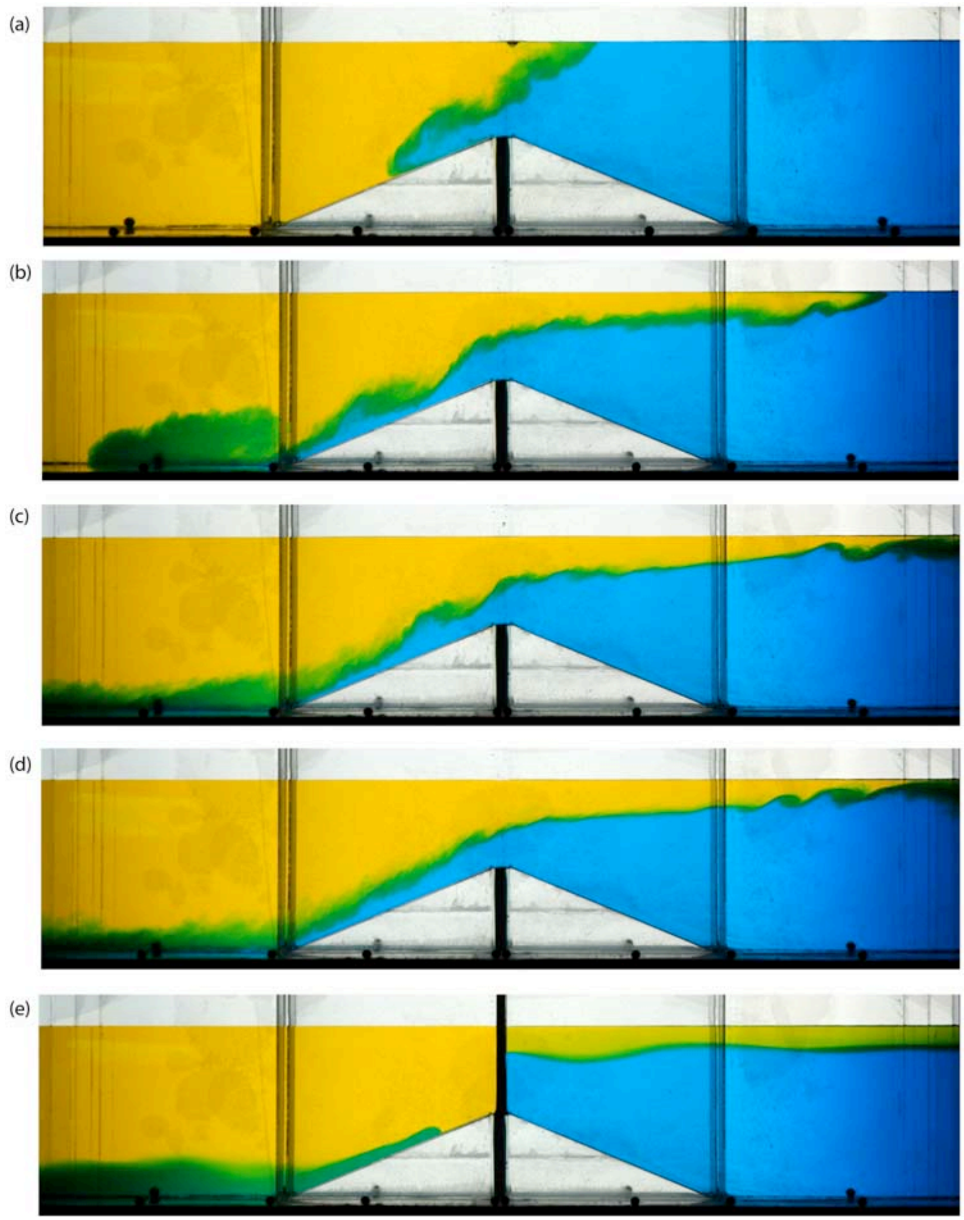


**Figure 3.** Photographs of the development of an exchange flow over the triangular sloping sill in an experiment with $H = 0.2$ m, $\Delta\rho/\rho_2 = 1.9\%$; $Re_L = 6.7 \times 10^4$; total duration of exchange flow 47 s. The vertical lines through the depth denote the extent of the constant width portion of the long lateral constriction, and the field of view is slightly wider than the total length of the constriction. Taken at times of (a) 2, (b) 6, (c) 19 and (d) 32 s, respectively, after withdrawal of the barrier. (e) Taken 54 s after replacing the barrier and showing the maximum runup on the slope of the bore reflected from the far left hand end of the channel. Figures 3c and 3d show the steady mean flow that represents most of the exchange period.

constant width to the right of the sill, the interface had a fixed slope that to first order reflected a balance of buoyancy and friction. At the larger Reynolds numbers there was continuous small-scale turbulence at the interface along the full length of the constriction (Figure 4a). In the experiments with smaller Reynolds numbers (Figure 4c) the billows and small-scale turbulence were more intermittent, and the mixing appeared to be relatively weak. In all cases the mixed water was continually carried away from the constriction into the two reservoirs. There were no billows along the stratified region above the gravity currents in the reservoirs, but there were billows on the head of each gravity current.

[21] After the barrier was reinserted, the gravity currents were reflected from the far ends of the channel as large-amplitude interfacial waves that involved no visible signs of further active mixing. When these waves arrived at the constriction they were reflected from the (now reinserted) barrier with a minor amount of overturning and stirring. Subsequently the wave motions caused no additional stirring of any consequence and all motions slowly decayed away.

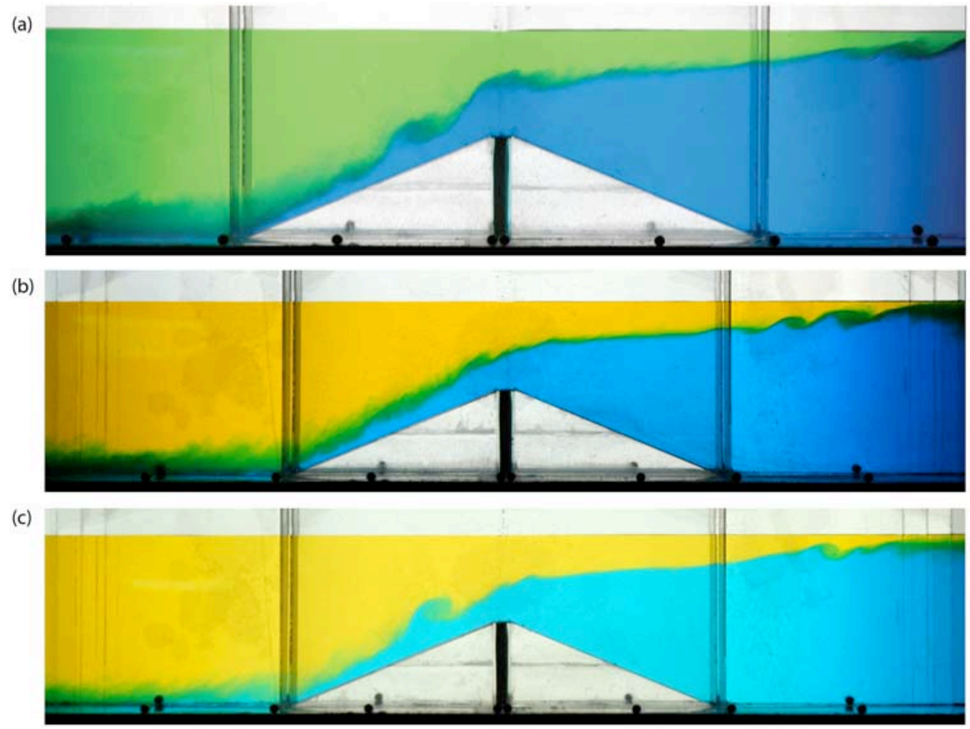


**Figure 4.** Images of flow through the constriction and over a triangular sloping sill for several different density contrasts, all with $H = 0.2$ m: (a) $\Delta\rho/\rho_2 = 7.9\%$ and $Re_L = 1.39 \times 10^5$ (run duration 20 s); (b) $\Delta\rho/\rho_2 = 1.9\%$ and $Re_L = 6.7 \times 10^4$; (c) $\Delta\rho/\rho_2 = 0.7\%$ and $Re_L = 4.2 \times 10^4$ (run duration 84 s). All images were taken while the mean flow was quasi-steady.

[22] In experiments with a vertical weir, the less dense fluid moved along the upper surface into the right reservoir while the dense fluid formed a jet that overshot and fell to the bottom on the left of the weir (Figure 5). The flow was accelerated on both sides of the weir in the exit regions of the constriction. Billows continually formed and overturned in these exit regions, collapsing into the mixed layer at the interface as they were advected past the end of the constriction.

[23] Experiments without topography are shown for comparison in Figure 6. These flows appear to be generally symmetric, with active turbulence along the length of the straight channel (where the constant interface slope here is primarily controlled by frictional effects). Acceleration of the layers occurs in the region where the channel width changes; the flow is subcritical beyond a hydraulic jump (which lies near the edges of the field of view in Figure 6).

## 4. Measurements

[24] Measurements of the free surface heights of the reservoirs before and after the exchange flows showed that the total volume of fluid in the reservoirs was conserved to within 0.01%. Control experiments reported by *Prastowo et al.* [2008] confirmed that the effects of the nonlinear equation of state lay within the uncertainty of the results reported below. Hence, we have assumed in all calculations that the density depends linearly on salinity.

[25] Examples of the final vertical profiles of density in each reservoir are plotted in Figure 7 for cases with the constriction and no bottom topography, the triangular sill and the weir. In each case the depth is normalized by the water depth and the density is normalized by the initial difference between reservoirs, and set to zero at the water surface. Once normalized in this way the profiles are approximately independent of the initial density difference and Reynolds number, as expected from the ideal hydraulic prediction (see below). There are significant differences between the profiles for a constriction alone and cases with a sill, primarily reflecting the change in mass transport. There is little difference in the right hand reservoir between those experiments with the two different sills. However, there are measurable differences between the profiles in the left reservoir for the weir (Figure 7c) and the triangular sill (Figure 7b), particularly close to the bottom boundary. These differences indicate that mixing is slightly greater in the left reservoir for the triangular sill case. We will further examine this asymmetry below, after first discussing the total amount of mixing in the channel.

[26] The focus of most work on strait and sill flows has been the rate of mass exchange. A lynch pin has been hydraulic theory for ideal two-layer flows having no mixing or friction, and from which the maximal mass transport through a contraction is predicted to be [e.g., *Ivey*, 2004]

$$M_{\max} = \frac{1}{4}\Delta\rho b_0 g'^{1/2} H^{3/2}, \quad (9)$$

where $g' = g\Delta\rho/\rho$. For exchange over a sill, (9) applies but with $H$ replaced by the water depth over the sill

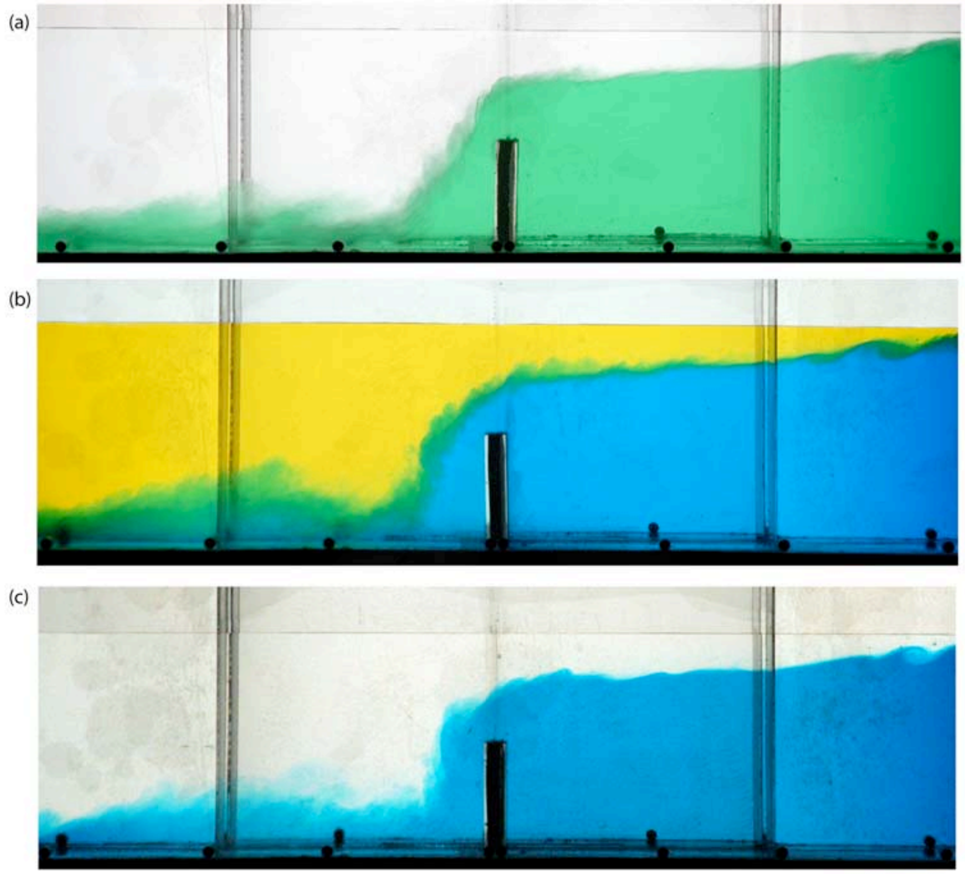


**Figure 5.** Images of flow through the constriction with a vertical-sided sill for several different density contrasts, all with $H = 0.2$ m: (a) $\Delta\rho/\rho_2 = 9.4\%$ and $Re_L = 7.6 \times 10^4$; (b) $\Delta\rho/\rho_2 = 4.8\%$ and $Re_L = 5.4 \times 10^4$; (c) $\Delta\rho/\rho_2 = 0.7\%$ and $Re_L = 2.0 \times 10^4$. All images were taken while the mean flow was quasi-steady.

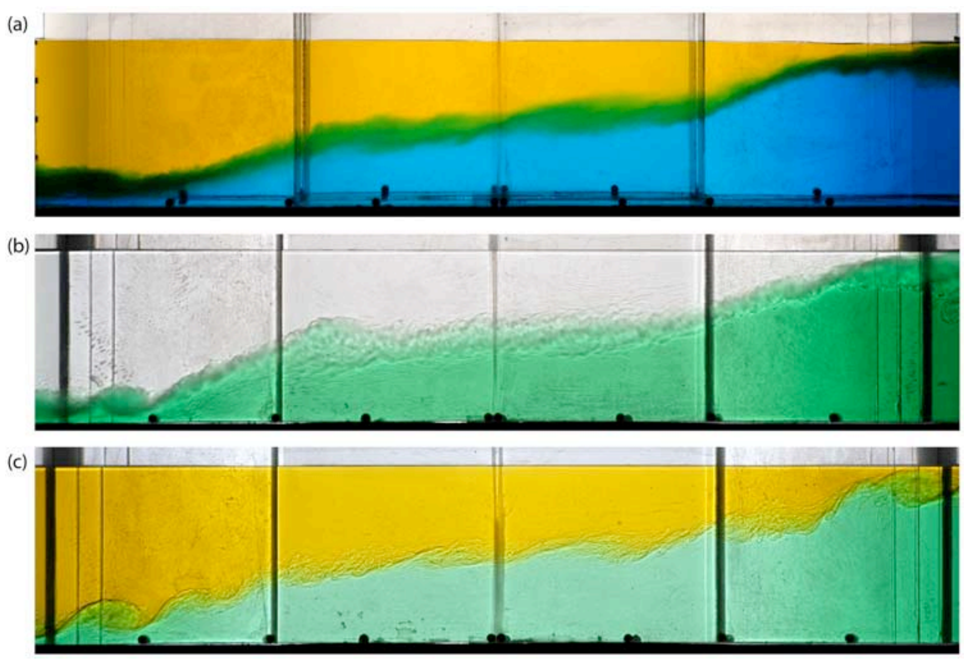


**Figure 6.** Images of flow through the long constriction for several different density contrasts, all with $H = 0.2$ m: (a) $\Delta\rho/\rho_2 = 9.2\%$ and $Re_L = 2.12 \times 10^5$ (run duration 16 s); (b) $\Delta\rho/\rho_2 = 3.0\%$ and $Re_L = 1.20 \times 10^5$; (c) $\Delta\rho/\rho_2 = 0.7\%$ and $Re_L = 5.8 \times 10^4$ (run duration 60 s). All images show the quasi-steady stage of the exchanges.

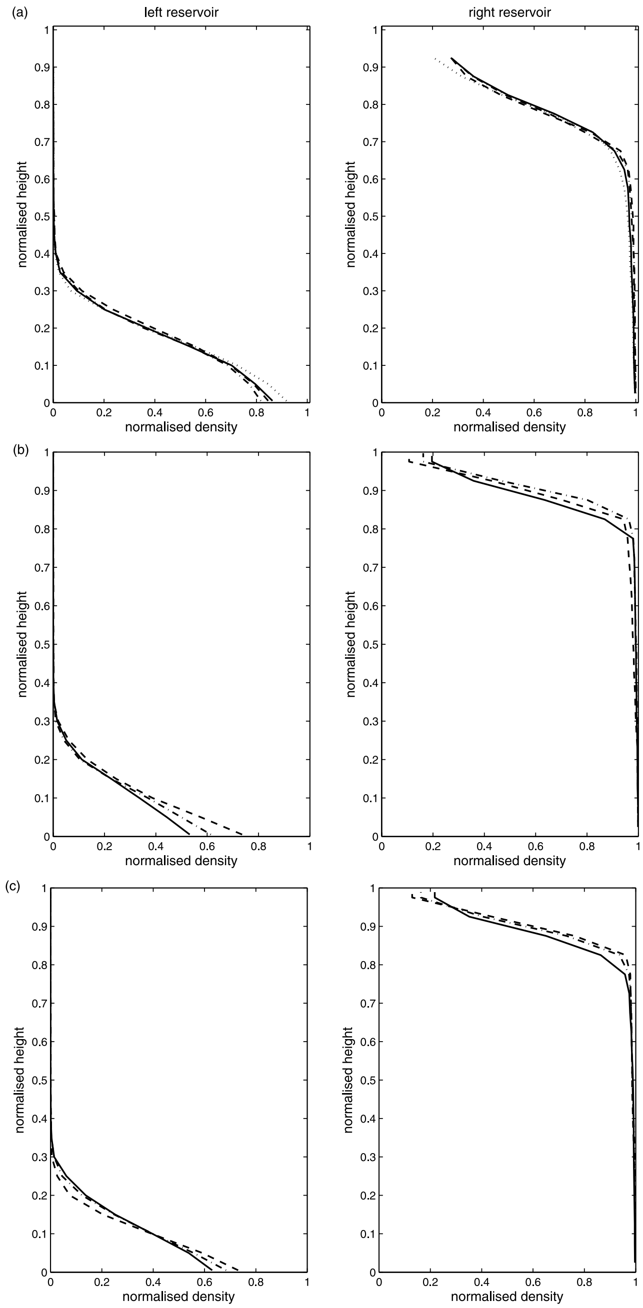


**Figure 7.** Profiles of the normalized density $(\rho(z) - \rho_1)/(\rho_2 - \rho_1)$ after exchange flows, plotted against normalized height $z/H$ for (a) the long constriction with no bottom topography, (b) the triangular sloping sill, and (c) the vertical weir. (left) Profiles in left reservoirs and (right) right reservoirs. Results in each case are plotted for three or four runs with different fractional density contrasts: In Figure 7a, $\Delta\rho/\rho_2 = 0.7\%$ (dotted line), 1.9% (solid line), 3.0% (dashed line) and 4.8% (dash-dotted line); in Figures 7b and 7c, $\Delta\rho/\rho_2 = 0.7\%$ (dashed line), 3.0% (dash-dotted line) and 9.5% (solid line). All cases had $H = 0.2$ m.

crest. The corresponding baroclinic volume exchange rate is $Q_{\max} = M_{\max}/\Delta\rho$.

[27] In the present experiments the net mass transport is readily obtained from the cumulative exchange during the period the barrier is open, determined from the density changes in each reservoir, divided by the flow duration $t_r$:

$$M_e = \frac{1}{t_r}\int_0^{h_1'} A(z)(\rho_1'(z) - \rho_1)\,dz. \tag{10}$$

*Prastowo et al.* [2008] reported that transport through short constrictions is 82% of the theoretical maximum while that through the long constriction used in the present experiments is 70% (±1%) of $M_{\max}$. Both results were independent of $Re_L$. Transport was also predicted to be reduced to 83% by mixing between the layers, and the remainder of the measured reduction was attributed to friction [see also *Winters and Seim*, 2000; *Gu and Lawrence*, 2005].

[28] Plots of $M_e/M_{\max}$ (Figure 8) show that this quantity remains independent of Reynolds number $Re_L$ for sill exchanges, even at the smaller Reynolds numbers. The measured normalized net mass transport over the weir is $M_e/M_{\max} = 0.74 \pm 0.01$ and for the triangular sill is $M_e/M_{\max} = 0.72 \pm 0.01$. The uncertainties in the measured transports are predominantly a result of the uncertainty in the experimental run time (±0.5 s in each case). These values are both significantly smaller than the transport predicted with mixing in the absence of friction, but slightly larger than that measured for the same long constriction, in which friction has a significant role. Recalling that the water depth $H/2$ over the sill replaces $H$ in the expression for the maximal

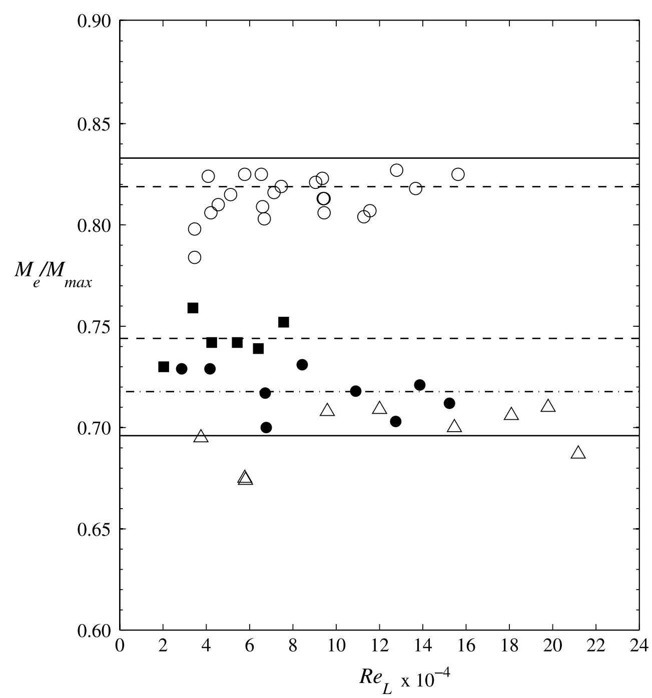


**Figure 8.** The normalized baroclinic mass transport as a function of the horizontal Reynolds number for the constriction with no bottom topography (open triangles), the weir (solid squares), and the sloping sill (solid circles). Data for the shorter, smoothly varying constriction with no bottom topography reported by *Prastowo et al.* [2008] (open circles) are included for comparison, along with the upper bound (upper solid line) predicted in that paper. Other lines show the mean values for each class of topography.

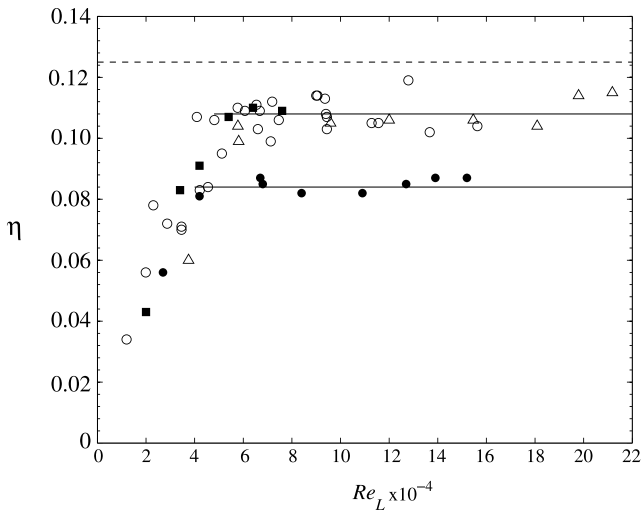


**Figure 9.** The measured mixing efficiencies $\eta$ as a function of the horizontal Reynolds number $Re_L$. Data for the long constriction, no bottom topography (open triangles), and short constrictions, no bottom topography (open circles) are compared with sill experiments: weir (solid squares); triangular sloping sill (solid circles). Solid lines are the average values for $Re_L > 5 \times 10^4$, the lower line for triangular sill runs and the upper line for all other runs.

transport (9) in the case of a sill, so that the transport is substantially smaller for a sill, we conclude that friction and mixing together lead to slightly less reduction of the normalized transport when a sill is added to a constriction, than they do in the case of a constriction with no topography.

## 5. Mixing Efficiency

[29] The calculated mixing efficiencies (8) for all runs are plotted in Figure 9. Here we show cases without topography using open symbols: the triangles show data from the longer constriction, while circles are from short channel experiments. The solid symbols are from experiments with bottom topography.

[30] The two cases without topography overlay accurately throughout the range of Reynolds number, and show that there is no dependence of the mixing on the length of the constriction. When plotted as a function of the depth-based Reynolds number instead of $Re_L$, the data from different constrictions do not collapse onto the same curve at the smaller Reynolds numbers. However, in either case it is clear that a constant mixing efficiency is reached at large values of the Reynolds number, making the choice of external parameter unimportant. From the combined data we determine the asymptotic cumulative efficiency to be $\eta = 0.108 \pm 0.01$ (mean deviation) for $Re_L > 5 \times 10^4$. This value for the efficiency includes a contribution from molecular diffusion during the 2 h allowed for motions to decay before density profiles were measured. However, diffusion is estimated theoretically (considering the extreme case of a density step) to have added much less than 0.005 to the result, hence is negligible compared with the random errors from other causes.

[31] The efficiencies for exchange flows over sills are also shown on Figure 9 using solid symbols. For the triangular sill (solid circles) the efficiency again increases with $Re_L$ and reaches a constant asymptote, again at $Re_L > 5 \times 10^4$. However, the asymptotic value $\eta = 0.084 \pm 0.003$ is slightly smaller than that with no bottom topography. We examined the uncertainty of these results by repeating a run with all conditions as identical as possible, and obtained a difference of 0.002 in the calculated efficiencies, which is comparable to the standard deviation ±0.003 of all the measurements at large $Re_L$. For the vertical weir (solid squares) the mixing efficiencies fall accurately on the same curve as those for no bottom topography, and reach the same asymptotic value, $\eta = 0.109$ at $Re_L > 5 \times 10^4$. Hence the presence of bottom topography does not necessarily play any role in influencing the amount of mixing. The smaller mixing efficiencies found for the triangular sill will be discussed below.

## 6. Discussion

[32] All of the exchange flows show different amounts of mixing in the left and right hand reservoirs. The contribution of each reservoir to the overall mixing efficiency in the flow cannot be identified because the amount of available potential energy released, $\Delta P_a$ (the denominator in (8)), cannot be unambiguously defined for each of the reservoirs separately. It is also not known how much kinetic energy was produced in each reservoir. However, the amount of mixing (6) in each reservoir can be evaluated. The mixing $P_{m_1}$ and $P_{m_2}$ in the left and right reservoirs, respectively, are

$$P_{m_1} = g\int_0^{h'_1} A\rho'_1(z)z\,dz - g\int_0^{h_{s1}} A\rho_2 z\,dz - g\int_{h_{s1}}^{h'_1} A\rho_1 z\,dz \qquad (11)$$

and

$$P_{m_2} = g\int_0^{h'_2} A\rho'_2(z)z\,dz - g\int_0^{h_{s2}} A\rho_2 z\,dz - g\int_{h_{s2}}^{h'_2} A\rho_1 z\,dz, \qquad (12)$$

where the variables are those defined in section 2.4.

[33] In Figure 10 we plot the average of the ratio $P_{m_1}/P_{m_2}$ over all runs having $Re_L > 5 \times 10^4$, for each of the constriction and sill geometries used in the present experiments and by *Prastowo et al.* [2008]. All cases (with the possible exception of the runs with the sloping sill) were asymmetric, such that there was a smaller amount of mixed water in the left reservoir, where the denser water intruded as a current against the rigid base, than in the right reservoir, where the less dense water intruded against the free surface. The greatest asymmetry occurred for the short constriction of smallest width ($b_o$ = 20 mm), where mixing in the left reservoir is about 60% of that in the right reservoir. The most symmetric case is the triangular sloping sill, where nearly the same amount of mixing occurred in both reservoirs.

[34] The cause of the asymmetry in the distribution of mixed water for constrictions with no topography is thought to be bottom friction (occurring in both the constriction and in the reservoir). Beginning with the short constriction case, a greater fraction of the turbulent kinetic energy is viscously dissipated at the base compared to that dissipated at the surface, leading to a smaller amount of mixing in the left reservoir than in the right reservoir. This effect will be greatest for the narrowest constriction, which generates the

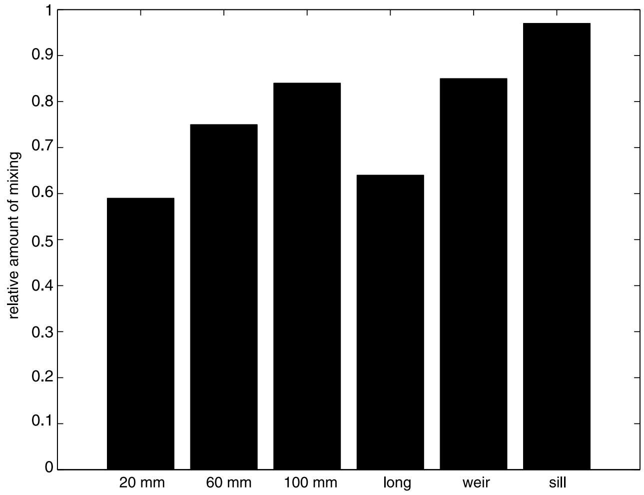


**Figure 10.** The potential energy change owing to mixing in the left reservoir relative to that in the right reservoir for six classes of experiment: for the short constriction reported by *Prastowo et al.* [2008] with $b_o$ = 20 mm, $b_o$ = 60 mm and $b_o$ = 100 mm and for the 1 m long, 60 mm wide constriction with no topography, the vertical weir, or the triangular sill. Each case shows the average ratio for all runs having $Re_L > 4 \times 10^4$ carried out in that class.

shallowest bottom current and brings the interfacial turbulence closest to the boundary. Similarly, for constrictions having the same width but different lengths (compare "60 mm" and "long" in Figure 10), the longer constriction gives the greater mixing asymmetry: the greater role of friction on the mean flow leads to a smaller transport and a thinner bottom current, hence greater viscous dissipation and less mixing. Sidewall viscous boundary layers in the constriction were shown, through runs with differing Reynolds numbers and constriction widths, to have negligible effects on mixing in the large Reynolds number regime [*Prastowo et al.*, 2008].

[35] When a sill is introduced into the long constriction (compare bars "weir" and "sill" with bar "long" in Figure 10), the data show that mixing in the left reservoir is increased and we attribute this to stronger turbulence induced by the dense overflow layer. This increased level of turbulence opposes the effect of bottom friction. Furthermore, the introduction of a sill produces a region on the right hand side of the channel, upstream of the sill, where turbulence is weak (see Figure 4). Thus, mixing in the right reservoir is reduced. Both influences tend to make the mixing on either side of the sill more symmetric. For the vertical weir these two influences approximately balance, perhaps coincidentally, leaving the overall amount of mixing and the bulk mixing efficiency unchanged relative to that with no bottom topography, as reported above. For the sloping sill the reduction of mixing on the right hand side owing to the dam effect is apparently larger than the increase owing to greater turbulence in the downslope gravity current (where the effect of bottom friction will come into play). The net result in this case is that the final change in potential energy owing to mixing is similar in both reservoirs while the overall amount of mixing is smaller than for the constrictions with no sill or the weir.

[36] The experiment design reported here leads to a measure of the cumulative amount of mixing. Only irreversible mixing is taken into account. The emphasis is on the whole of the exchange process, rather than on a specific mixing mechanism, and the mean flows are in all cases hydraulically controlled. Mechanisms that play a role in mixing in these exchange flows are (1) shear instability, leading to growth and collapse of Kelvin-Helmholtz billows, within the constriction, (2) stationary hydraulic jumps at the exits from the constriction, (3) Kelvin-Helmholtz billows on the interface, and lobe and cleft instabilities on the rigid base, at the head of the gravity currents as they propagate across each reservoir, (4) overturning during the reflections of these gravity currents at the end walls of the channel and in subsequent reflections of internal waves at the barrier and end walls, and (5) subsequent very small mixing events due to wave-mean shear or wave-wave interactions in the interior of the stratified reservoirs while motions are decaying away. These processes are all generic to the strait-basin configuration and will be present in geophysical exchange flows (with the possible exception of gravity current heads and their interaction with the end wall, the heads being absent in the special case of steady long-lived exchange flows). On the other hand, our qualitative observations indicate that most of the above mechanisms contributed little to the net amount of mixing. The most intense mixing took place within the constriction and at the exits, and the mixed (or stirred) water was advected away into the reservoirs.

[37] Although it is not possible to measure the separate contributions to mixing of the various processes in the exchange flows, we use a scaling analysis to estimate the contribution of the gravity current heads. The flow in the constriction releases available potential energy at the rate $\dot{P}_S \sim gM_eH$. Propagation of the gravity currents releases available potential energy at the rate $\dot{P}_G \sim gM_ed$, $d$ is the height of the currents. Thus $\dot{P}_G/\dot{P}_S \sim d/H < 1/6$ for the experiments reported here. In other experiments with no constriction we have found that the gravity current exchange gives a mixing efficiency of $\eta_G \approx 0.06$, and a similar value was found in numerical experiments [*Ozgokmen et al.*, 2009], although the mixing in this type of flow is again dominated by billows in the central region of the channel at early stages of the exchange. Because the corresponding rates of mixing are $m_S = \dot{P}_S\eta$ and $m_G = \dot{P}_G\eta_G$, we find $m_G/m_S < 0.1$. This result is consistent with previous conclusions that there is negligible dissipation of energy from the mean flow in gravity currents [*Shin et al.*, 2004]. It also implies that, if the gravity current mixing were absent, we would find $\eta < 0.12$ for the exchange flow, no more than 10% larger than the measured overall value.

[38] The laboratory results clearly reach an asymptotic value at the larger Reynolds numbers achieved. Hence the results should be applicable to oceanic exchanges having much greater Reynolds numbers. As the experiment design yields the net result of the sustained shear and turbulent mixing, the cumulative efficiency is also likely to be relevant to a broader range of two-layer stratified shear flows, where Kelvin-Helmholtz billows are the dominant mechanism causing mixing. The mixing efficiency found here may provide a better description of the time- and space-averaged mixing relevant to the large-scale ocean dynamics. If the ocean-wide average of mixing efficiency is 10% (just half of

that which is commonly assumed), then a revision of the ocean energy budget is necessary; in particular one must question whether the power required to sustain a steady circulation of the type proposed by *Munk and Wunsch* [1998] is available. On the other hand, it has been argued [*Hughes and Griffiths*, 2006] that entrainment into the sinking regions of the overturning circulation (turbulent slope currents) has global effects that reduce, by a factor of between three and ten, the *Munk and Wunsch* [1998] estimate for the total amount of mixing required to maintain the observed overturning. These two results together potentially allow a smaller reduction (by a factor of between 1.5 and 5) in the required energy input. However, the real point is that the energy budget is not well constrained because the conversion rate of kinetic to available potential energy is uncertain. The mixing efficiency given by the present experiments is remarkably insensitive to conditions, and its integrative nature lends greater reliability. However, mixing efficiency is not likely to take one universal value and more work is required.

[39] The more detailed examination of potential energy changes in each reservoir reveal additional information about the dependence of mixing on geometry and topography that may be relevant to ocean exchange flows. In particular, the presence of a sill tends to decrease the energy that goes into mixing the density field in the dense reservoir side of the sill. There is not a matching increase in mixing in the downslope current produced by the dense overflow, where bottom friction causes greater dissipation. Therefore the overall amount of mixing is smaller for a sill with sloping sides than for any of the other cases considered.

## 7. Conclusions

[40] The cumulative amount of mixing in hydraulically controlled exchange flows can be measured accurately from density profiles after a finite period of flow. The amount of mixing, specified as a mixing efficiency, is remarkably insensitive to the geometry of the constriction and bottom topography. It is dependent on the Reynolds number based on the horizontal length scale characterizing the flow acceleration, up to a well-defined transition beyond which the efficiency attains a constant value. We find a cumulative efficiency $\eta$ = 0.11 (±0.01) at Reynolds number, $Re_L > 5 \times 10^4$. This result is consistent with the predicted upper bound on the mixing efficiency of $\eta$ = 0.125 obtained from a simple scaling analysis of *Prastowo et al.* [2008]. The results indicate that, if there is any dependence of the mixing on the shape of the topography, then only smaller values of the efficiency are possible. The smallest cumulative mixing efficiency found at large Reynolds numbers, $\eta$ = 0.08, was for the case of a sill that produced a dense overflow down a gentle slope.

[41] These measured mixing efficiencies are similar to a theoretical value $\eta$ = 0.11 found by *Arneborg* [2002], who considered the net result of a localized turbulent mixing event with a maximum efficiency of 0.2 followed by the subsequent spreading of the mixed patch. However, our results are smaller than the equivalent cumulative efficiency $\eta$ = 0.15 found in computational modeling of a single Kelvin-Helmholtz billow [*Caulfield and Peltier*, 2000; *Peltier and Caulfield*, 2003], and smaller than the maximum mixing efficiency of $\eta \sim 0.2$ measured in a range of other experiments [*Rohr et al.*, 1984; *Ivey and Imberger*, 1991; *Monti et al.*, 2007] and often assumed in discussions of global ocean energy balances [*Webb and Suginohara*, 2001; *Wunsch and Ferrari*, 2004].

[42] We have considered only the case of sills with heights one half of the full depth of the basin. Further work might examine the case of a broad sill with no lateral constriction, and whether the mixing behavior for a sloping sill varies with sill height, especially when the height is greater than $H$/2, which reduces the depth of the exchange flow and increases the height of fall for the dense overflow.

[43] **Acknowledgments.** We thank Tony Beasley for construction of the laboratory apparatus. T.P. acknowledges the Australian Government for the award of an AusAid scholarship and the Directorate General of Higher Education, Ministry of National Education, Republic of Indonesia, for the award of a PAR C scholarship. The work was also supported by the Australian Research Council (grant DP0664115).

## References

Arneborg, L. (2002), Mixing efficiencies in patch turbulence, *J. Phys. Oceanogr.*, *32*, 1496–1506, doi:10.1175/1520-0485(2002)032<1496:MEIPT>2.0.CO;2.

Bryden, H. L., and A. J. G. Nurser (2003), Effects of strait mixing on ocean stratification, *J. Phys. Oceanogr.*, *33*, 1870–1872, doi:10.1175/1520-0485(2003)033<1870:EOSMOO>2.0.CO;2.

Caulfield, C. P., and W. R. Peltier (2000), The anatomy of the mixing transition in homogeneous and stratified free shear layers, *J. Fluid Mech.*, *413*, 1–47, doi:10.1017/S0022112000008284.

Ellison, T. H. (1957), Turbulent transport of heat and momentum from an infinite rough plane, *J. Fluid Mech.*, *2*, 456–466, doi:10.1017/S0022112057000269.

Farmer, D. M., and L. Armi (1986), Maximal two-layer exchange flow over a sill and through the combination of a sill and contraction with barotropic flow, *J. Fluid Mech.*, *164*, 53–76, doi:10.1017/S002211208600246X.

Gargett, A. E., and J. N. Moum (1995), Mixing efficiencies in turbulent tidal fronts: Results from direct and indirect measurements of density flux, *J. Phys. Oceanogr.*, *25*, 2583–2608, doi:10.1175/1520-0485(1995)025<2583:MEITTF>2.0.CO;2.

Gu, L., and G. A. Lawrence (2005), Analytical solution for maximal frictional two-layer exchange flow, *J. Fluid Mech.*, *543*, 1–17, doi:10.1017/S0022112005006002.

Hughes, G. O., and R. W. Griffiths (2006), A simple convective model of the global overturning circulation, including the effects of entrainment into sinking regions, *Ocean Modell.*, *12*, 46–79, doi:10.1016/j.ocemod.2005.04.001.

Ivey, G. N. (2004), Stratification and mixing in sea straits, *Deep Sea Res., Part II*, *51*, 441–453, doi:10.1016/j.dsr2.2003.07.020.

Ivey, G. N., and J. Imberger (1991), On the nature of turbulence in a stratified fluid. Part I: Energetics of mixing, *J. Phys. Oceanogr.*, *21*, 650–658, doi:10.1175/1520-0485(1991)021<0650:OTNOTI>2.0.CO;2.

Ivey, G. N., K. B. Winters, and J. Koseff (2008), Density stratification, turbulence, but how much mixing?, *Annu. Rev. Fluid Mech.*, *40*, 169–184, doi:10.1146/annurev.fluid.39.050905.110314.

Linden, P. F. (1979), Mixing in stratified fluids, *Geophys. Astrophys. Fluid Dyn.*, *13*, 3–23, doi:10.1080/03091927908243758.

Linden, P. F. (1980), Mixing across a density interface produced by grid turbulence, *J. Fluid Mech.*, *100*, 691–703, doi:10.1017/S002211208000136X.

Monti, P., G. Querzoli, A. Cenedese, and S. Piccinini (2007), Mixing properties of a stably stratified parallel shear layer, *Phys. Fluids*, *19*, 085104, doi:10.1063/1.2756580.

Moum, J. N. (1996), Efficiency of mixing in the main thermocline, *J. Geophys. Res.*, *101*, 12,057–12,069, doi:10.1029/96JC00508.

Munk, W., and C. Wunsch (1998), Abyssal recipes II: Energetics of tidal and wind mixing, *Deep Sea Res., Part I*, *45*, 1977–2010, doi:10.1016/S0967-0637(98)00070-3.

Osborn, T. R. (1980), Estimates of the local rate of vertical diffusion from dissipation measurements, *J. Phys. Oceanogr.*, *10*, 83–89, doi:10.1175/1520-0485(1980)010<0083:EOTLRO>2.0.CO;2.

Ozgokmen, T. M., T. Iliescu, and P. F. Fischer (2009), Large eddy simulation of stratified mixing in a three-dimensional lock-exchange system, *Ocean Modell.*, *26*, 134–155, doi:10.1016/j.ocemod.2008.09.006.

Patterson, M. D., C. P. Caulfield, J. N. McElwaine, and S. B. Dalziel (2006), Time dependent mixing in stratified Kelvin-Helmholtz billows: Experimental observations, *Geophys. Res. Lett.*, *33*, L15608, doi:10.1029/2006GL026949.

Peltier, W. R., and C. P. Caulfield (2003), Mixing efficiency in stratified shear flows, *Annu. Rev. Fluid Mech.*, *35*, 135–167, doi:10.1146/annurev.fluid.35.101101.161144.

Prastowo, T., R. W. Griffiths, G. O. Hughes, and A. M. Hogg (2008), Mixing efficiency in controlled exchange flows, *J. Fluid Mech.*, *600*, 235–244, doi:10.1017/S0022112008000554.

Rohr, J. J., E. C. Itsweire, and C. W. Atta (1984), Mixing efficiency in stably stratified decaying turbulence, *Geophys. Astrophys. Fluid Dyn.*, *29*, 221–236, doi:10.1080/03091928408248190.

Ruddick, B., D. Walsh, and N. Oakey (1997), Variations in apparent mixing efficiency in the North Atlantic Central Water, *J. Phys. Oceanogr.*, *27*, 2589–2605, doi:10.1175/1520-0485(1997)027<2589:VIAMEI>2.0.CO;2.

Shin, J. O., S. B. Dalziel, and P. F. Linden (2004), Gravity currents produced by lock exchange, *J. Fluid Mech.*, *521*, 1–34, doi:10.1017/S002211200400165X.

St. Laurent, L., and H. Simmons (2006), Estimates of power consumed by mixing in the ocean interior, *J. Clim.*, *19*, 4877–4890, doi:10.1175/JCLI3887.1.

Stigebrandt, A., and J. Aure (1989), On vertical mixing in the basin waters of fjords, *J. Phys. Oceanogr.*, *19*, 917–926, doi:10.1175/1520-0485(1989)019<0917:VMIBWO>2.0.CO;2.

Webb, D. J., and N. Suginohara (2001), Vertical mixing in the ocean, *Nature*, *409*, 37, doi:10.1038/35051171.

Winters, K. B., and H. E. Seim (2000), The role of dissipation and mixing in exchange flow through a contracting channel, *J. Fluid Mech.*, *407*, 265–290, doi:10.1017/S0022112099007727.

Wunsch, C., and R. Ferrari (2004), Vertical mixing, energy, and the general circulation of the oceans, *Annu. Rev. Fluid Mech.*, *36*, 281–314, doi:10.1146/annurev.fluid.36.050802.122121.



R. W. Griffiths, A. M. Hogg, G. O. Hughes, and T. Prastowo, Research School of Earth Sciences, Australian National University, Canberra, ACT, 0200, Australia. (Ross.Griffiths@anu.edu.au; Andy.Hogg@anu.edu.au; Graham.Hughes@anu.edu.au; t_prastowo@yahoo.com)